Initial contact and toe-off event detection method for in-shoe motion sensor

Chenhui Huang, Kenichiro Fukushi, Zhenwei Wang, Hiroshi Kajitani, Fumiyuki Nihey and Kentaro Nakahara

Abstract Initial contact (IC) and toe-off (TO) events are tools for measuring and analyzing human gait. As a simpler method for detecting gait events that depends only on inertial measurement unit (IMU) signals is needed, in this study, we propose a simpler signal feature-based method for detecting gait events that is feasible for use in-shoe motion sensor (IMS) systems, and these exact features are used to determine the timing of IC and TO according to biomechanical knowledge. We then evaluate the precision of the method. Twenty-six healthy subjects were recruited to participate in experiments, during which an IMS along with a Vicon 3-D motion analyzer were applied to measure the trajectory of the foot and to judge the IC and TO timing. Temporal features of the foot to ground kinematic waveform at the time of IC and TO are newly discovered by synchronizing the two systems. The temporal precision of an algorithm for automatic IC and TO detection is evaluated on the basis of root

Chenhui Huang
Biometrics Research Labs., NEC Coporation, Hinode 1131, Abiko, 270-1174, Japan, e-mail: chenhui.huang@nec.com

Kenichiro Fukukshi
Biometrics Research Labs., NEC Coporation, Hinode 1131, Abiko, 270-1174, Japan, e-mail: k-fukushi@nec.com

Zhenwei Wang
Biometrics Research Labs., NEC Coporation, Hinode 1131, Abiko, 270-1174, Japan, e-mail: w-zhenwei@nec.com

Hiroshi Kajitani
Biometrics Research Labs., NEC Coporation, Hinode 1131, Abiko, 270-1174, Japan, e-mail: h-kajitani@nec.com

Fumiyuki Nihey
Biometrics Research Labs., NEC Coporation, Hinode 1131, Abiko, 270-1174, Japan, e-mail: nihey@nec.com

Kentaro Nakahara
Biometrics Research Labs., NEC Coporation, Hinode 1131, Abiko, 270-1174, Japan, e-mail: k-nakahara@nec.com

mean square error (RMSE) and intraclass correlation coefficient (ICC). The RMSE of the TO detection was 1.22%, and that of the IC was 1.40%. The ICC of the TO detection was 0.7011, and that of the IC was 0.7721. The results demonstrate the high detection accuracy and reliability of this simpler IC and TO automatic detection algorithm for IMSs.

1 Introduction

The relationship between health and walking can be revealed by gait analysis in the laboratory in order to diagnose certain neurological diseases and to detect and predict falls [1-4]. A gait event is defined by the timing or phase of a gait cycle, and by determining initial contact (IC) and toe-off (TO) events, a gait cycle is divided into a stance phase and swing phase [5]. Previous reports indicated that using information for different gait phases can bring additional insight into practical gait assessment such as for Parkinson's disease and osteoarthritis. [6-7]. Determining gait event timing is conventionally done using force plate data and visual foot-switching recording, or by using a 3-D motion analysis system in a laboratory [8-9].

Recently, inertial measurement units (IMUs) have been applied for gait analysis outside the laboratory [10-14]. Integrating a motion sensor into a shoe, which can be called an "in-shoe motion sensor (IMS) system," is considered to be a solution for achieving gait analysis in daily life [15-16]. With this system, foot motion, i.e., foot to ground kinematic information, which is a part of gait, can be measured in real time, and the data can be transmitted to a smartphone. To analyze gait in detail in daily life, a method for detecting gait events with an IMS system is needed.

Stamataki et al. [12] proposed detecting gait events by selecting thresholds in gait signals taken from the instep. However, the threshold values are highly dependent on individual differences or walking velocity, and fixed thresholds are difficult to cover for all subjects; thus, the precision and reliability of gait-event detection will be limited. Detecting gait events by using kinematic signal patterns is considered to be a solution for raising the precision and reliability. Mannini et al. [14] determined gait events by inputting instep-measured gait-signal patterns into a hidden Markov model (HMM), and Mijailovic et al. [17] suggested detecting gait events with artificial neural networks. However, constructing detection models such as with HMM or artificial neural networks, which are machine learning methods, requires collecting big data and making complicated calculations.

Although using kinematic signal patterns to detect gait events is considered promising, a simpler detection method for IMS systems is needed. In this study, we try to achieve this goal by determining signal patterns according to conventional biomechanical knowledge. At the timing of a gait event, especially when IC and TO occur, the muscle and joint activity patterns instantaneously transition from one to another [5, 18]. Every kinematic signal pattern in gait signals should be intrinsically induced by the human walking mechanism. Therefore, we consider the features of IC and TO to be significant turning points like peaks or valleys in signal

waveforms, which are easy to recognize. The timing of IC and TO can be determined by specifying these features from signal waveforms.

In this study, we apply a 3-D motion analysis system as a reference rater and first try to specify the exact features of IC and TO from IMS gait signals. Second, we use these exact features to determine the timing of IC and TO. Third, we evaluate the precision of the method.

2 Material and Method

2.1 Definition of gait cycle

Commonly, a gait cycle is defined as a periodic motion starting from the timing of an initial contact (IC) on the ground to the next IC, and a gait cycle is divided into a stance phase and swing phase, which occupy 60% and 40% of one gait cycle, respectively. At the timing of IC, the gait transitions from the swing phase to stance phase, and at the timing of TO, the gait transitions from the stance phase to swing phase. In the most common case, an IC event occurs at 0

IC is a dynamic process in which instantaneous foot motion alteration occurs before and after it, and a potential feature likely appearing around IC may be split apart under the conventional definition of gait cycle division. It has been observed that dynamic foot motion is interrupted when the foot is flat during the middle of the stance phase, where the foot sole has completely landed and is static relative to the ground. For our goal, partitioning a gait cycle from the middle of a stance phase to the next middle of a stance phase to reserve all potential features in one cycle is considered promising. Therefore, in this study, we shift the start and end of the gait cycle to the beginning of the terminal stance phase and the end of the mid-stance phase in gait analysis, respectively. Figure 1 shows the defined gait phases and events in one gait cycle in this study. This way, a TO event shifts to around 30%, and an IC shifts to around 70% of a gait cycle.

2.2 Subjects

Twenty-six subjects, that is, 20 males and 6 females, participated in the study. The subjects' data, including sex, age, height, weight, and shoe size, were collected. The average age was 39.3 ± 9.5 years, the average height was 169.5 ± 7.7 cm, the average weight was 67.2 ± 12.1 kg, and the average shoe size was 26.4 ± 1.0 cm. All subjects could walk independently without any assistance devices such as canes, crutches, or orthotic devices. They had normal or corrected-to-normal vision, no history of neuromuscular or orthopedic diseases, and no obstacles in communication. The experimental procedure was explained to all subjects, and informed consent was

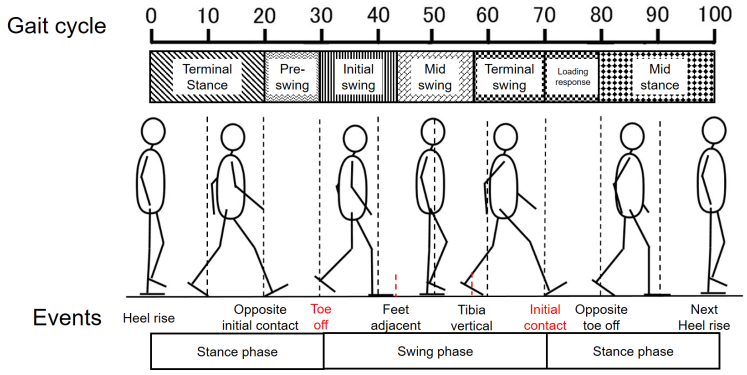

Fig. 1 Defined gait phases and events in one gait cycle. Start and end are shifted to the beginning of terminal stance: TO shifts to around 30% and IC to around 70% of the gait cycle.

obtained individually before the experiment. The study was approved by the Local Ethics Committee.

2.3 Experimental environment

Fig. 2 shows the scheme of the experimental environment and setup. An IMS was mounted on an insole that was placed under the foot arch to prevent discomfort during walking. The insole was inserted into a shoe. To assure that all subjects could walk in a natural way, sports shoes matched to individual foot size were chosen for the experiment. The IMS was worn only on the right foot. The data measured by the IMS was transferred to a smartphone interface and stored. Here, of the three accelerometer axes, the X-axis is defined as the left-right direction (left: +, right: -), the Y-axis is defined as the anterior-posterior direction (posterior: +, anterior: -), and the Z-axis is defined as the superior-inferior direction (superior: +, inferior: -).

A 3-D motion analysis system, Track 3 (Vicon Motion Systems, UK), was used for obtaining the trajectory of the feet. The motion analysis space was partitioned by 10 motion-capture cameras, Bonita B10 (Vicon Motion Systems, UK), fixed at a height of 2.5 m from the ground. The cameras were set on both sides of a straight walking path, five cameras on each side. The vertical distance from the median line to each side was 3 m, and the distance between cameras on each side was 2 m. Markers for motion capture were attached to the surface of the shoe as shown in Fig. 2; one marker was located at the toe, and the others were at the middle and back of the foot (four can be seen in Fig. 2, with two others hidden on the opposite side). The traced trajectories of the toe marker were used to clarify the moment of a TO event.

Considering that there is little deformation from the heel to the metatarsophalangeal joint of the foot during walking, the deformation can be ignored in macro-

measurement. Therefore, this part of the foot can be considered as a rigid body, and markers concentrated at the middle and the back of the foot can be used for composing a rigid body in the Vicon system. The gravity center of the composed rigid body was set the same as the position of the heel; thus, the motion of the rigid body was equivalent to the motion of the middle and back of the foot. Also, the trajectory of the gravity center was equivalent to the trajectory of the heel, could can be used to clarify the moment of an IC.

The subjects walked 8 m straight along the pathway, which was about 0.8-m wide. The subjects were then asked to walk four successive trials along the pathway at a self-determined comfortable speed. Before the data collection, subjects were given a 2-min practice session to familiarize themselves with the environment and procedure. In every trial, the subjects walked in a round trip, but only one way was recorded in order to avoid signal distortion in the system due to the turn-around motion in the trial. The data sampling frequency of the Vicon system and of the IMS were both set at 100 Hz.

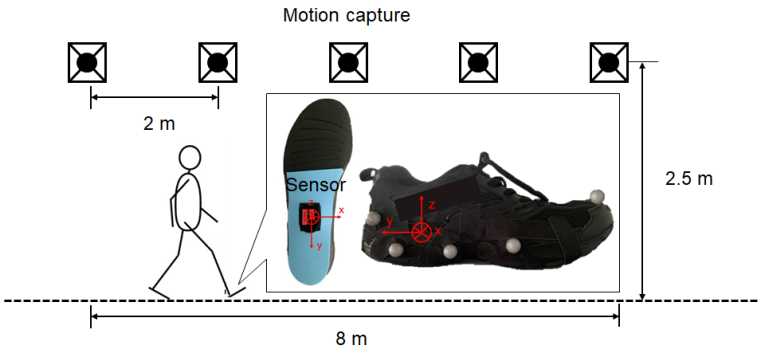

Fig. 2 Scheme of experimental environment and setup.

2.4 Data processing and synchronization

The Vicon system and the IMS operated independently, which means that the data collection starting times were not simultaneous. For gait-event detection in this research, signals acquired by the Vicon system and the IMS needed to be completely synchronized. In our experiment, there was no hardware connection between the two systems; instead, a software synchronization method was chosen here that superposes signals of similar physical quantity taken by different instruments with data processing software. However, while the Vicon system is able to record the position of the markers/rigid body and the Euler angle of the rigid body relative to the earth, the IMS can measure only the acceleration and angular velocity relative to

the IMS coordinate system. This means that the physical quantities acquired by the two instruments were completely different, so the software synchronization method could not be applied immediately here.

It has been noted that the Euler angle can be obtained by inputting the acceleration and angular velocity into a Madgwick filter [19]. The process of calculating the Euler angle with the Madgwick filter can be expressed by Equations (1) to (4).

$$q_{0,1,2,3} = M(Acc_{x,y,z}\ , Gyro_{roll\ ,pitch\ ,yaw}) \tag{1}$$

$$E_{roll} = \tan^{-1}(\frac{q_0 q_1 + q_2 q_3}{0.5 - q_1^2 q_2^2}) \times \frac{180}{\pi} \tag{2}$$

$$E_{pitch} = 2\sin^{-1}(q_0 q_2 - q_1 q_3) \times \frac{180}{\pi} \tag{3}$$

$$E_{yaw} = \tan^{-1}(\frac{q_1 q_2 + q_0 q_3}{0.5 - q_2^2 q_3^2}) \times \frac{180}{\pi} \tag{4}$$

, where M means the Madgwick filter operator, $q_{0,1,2,3}$ defines the four output quaternions, $Acc_{x,y,z}$ defines the input three-axis acceleration value, $Gyro_{roll,pitch,yaw}$ defines the input three-axis angular velocity value, and E_{roll}, E_{pitch}, E_{yaw} are the calculated Euler angles. Then, synchronization becomes possible by using Euler angle waveforms of both systems.

Regarding the definition of axis direction, the rotation of the X-axis means the alteration of the sole-to-ground angle in the dorsal-flexion/plantar-flexion (SGADP) direction, the rotation of the Y-axis means the alteration of the sole-to-ground angle in the pronation-supination (SGAPS) direction, and the rotation angle of the Z-axis means the alteration of the sole-to-ground angle in the abduction-adduction (SGAAA) direction. It was found that the waveform of SGADP at the beginning of a walking trial [shown in Fig. 3(a) in red dashed circles] was different from white noise/random motion and walking at a uniform velocity. Thus, this part of the waveform could be utilized for synchronizing the two signals acquired from the different systems.

First, a window was set on this particular part of the IMS waveform. Then, it was shifted on the temporal axis until it was completely superposed on the same part of the Vicon waveform. The superposing position was judged on the basis of the appearance of the maximum Pearson product-moment correlation coefficient between the two waveforms. After synchronization [see Fig. 3(b)], the data streams were split stride by stride grossly from the middle stance phase to the next one. Due to an occasionally weak Bluetooth connection between the IMS sensor and smartphone user interface, data packets were lost during communication, which

induced tiny deviations between the IMS and Vicon waveforms in the later part of the data stream. Therefore, after splitting the data stream, the waveforms of each stride of the IMS and Vicon were synchronized again by making their peaks and valleys in the SGADP waveform uniform.

The directly measured $Acc_{x,y,z}$ and $Gyro_{roll\ ,pitch\ ,yaw}$ are values relative to the coordinate system on the IMS. However, relative to the earth, the three coordinate axes of the IMS are always changing due to the rotation of the ankle joint during walking. The directly measured $Acc_{x,y,z}$ needs to be transformed into an inertial coordinate system. The transformation process can be expressed by Eqs. (5) to (6).

$$R = \begin{bmatrix} 2(q_0^2 + q_1^2) - 1 & 2(q_1q_2 + q_0q_3) & 2(q_1q_3 - q_0q_2) \\ 2(q_1q_2 - q_0q_3) & 2(q_0^2 + q_2^2) - 1 & 2(q_2q_3 + q_0q_1) \\ 2(q_1q_3 + q_0q_2) & 2(q_2q_3 + q_0q_1) & 2(q_0^2 + q_3^2) - 1 \end{bmatrix} \tag{5}$$

$$Acc^*_{x,y,z} = R^{-1} \times Acc_{x,y,z} \tag{6}$$

, where R means the coordinate transformation operator, and $Acc^*_{x,y,z}$ means the foot acceleration vector relative to the earth. Then, a second-order low-pass Butterworth filter was used to filter the kinematic data (cut-off frequency of 10 Hz).

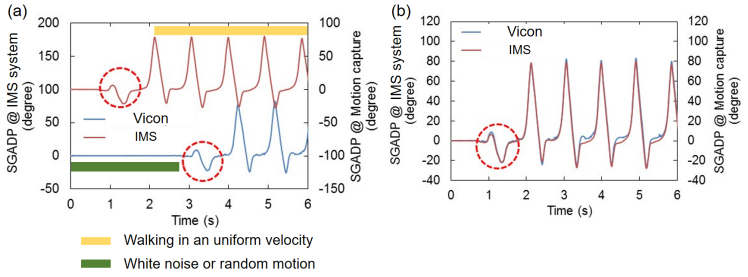

Fig. 3 Examples of two SGADP waveforms measured by motion capture and IMS. (a) Starting time was not simultaneous; (b) synchronization result after using specific waveform shape at beginning of stride.

2.5 Automatic TO and IC detection

In this study, all parts of the data processing were executed on MATLAB (MathWorks, USA). As shown in Fig. 4, the timing of TO (T_{TO}) and IC (T_{IC}) were the minimum positions in the trajectories in the gravity direction. The offset appearing at the middle of the stance phase (at a 0% gait cycle) was induced by the height of

the selected marker. Then, the temporal features of the TO and IC could be specified from the synchronized IMS waveform at T_{TO} and T_{IC}. These features 1) existed in each subject ' s data, 2) were easy to recognize, and 3) allowed us to generate an automatic algorithm for detecting TO and IC. They were selected from nine obtained types ($Acc^{*}_{x,y,z}$, $Gyro_{roll,pitch,yaw}$, and $E_{roll,pitch,yaw}$) of waveforms. Here, we focus on some features on Y and Z acceleration waveforms.

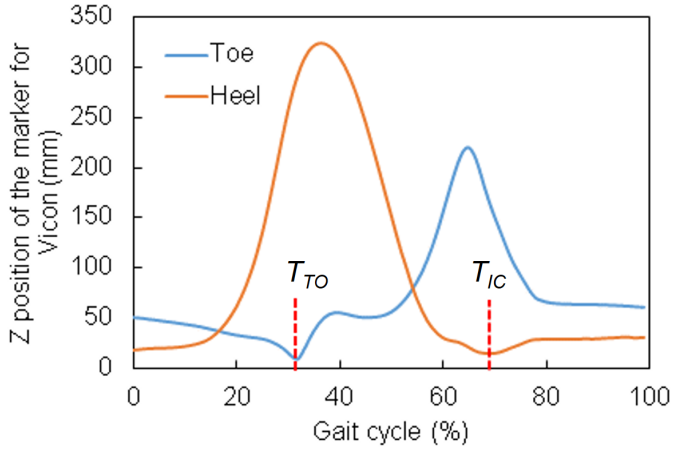

Fig. 4 Timing of IC and TO.

2.5.1 TO detection

An example of synchronized Y and Z acceleration waveforms L_y and L_z and the trajectory in the Z direction of the marker on the toe are combined in Fig. 5(a) and (c), and the synchronized angular velocity waveform in the dorsi-plantarflexion direction L_{gx} and the trajectory in the Z direction of the marker on the toe are combined in Fig. 5(b) and (d). A double valley with a "W" shape appeared in the Y acceleration waveform around the timing of T_{TO}, and the peak between the valleys in the "W" seemed to just match the timing of T_{TO}. Here, we marked the three turning points in "W" as V_{ya}, V_{yb}, and P_{ya} as shown in Fig. 5(a), respectively. In addition, around T_{TO}, a peak and a valley appeared in the Z acceleration waveform, and a peak appeared in the angular velocity waveform in the dorsi-plantarflexion direction, which are marked as P_{za}, V_{za} and P_{gxa}, respectively. Which one is the prospective feature of TO cannot be ascertained at this stage, but it is thought to be highly possible for the prospective feature to appear around this range. To ascertain the exact prospective feature, the obvious features (total number of candidate features set to N) are taken from the waveform as candidates; then, the temporal deviation between T_{TO} and the timing of each of the features is evaluated, and the smallest one

will be the prospective feature as a result. As a summary, a flow chart for determining the prospective feature is shown in Fig. 6.

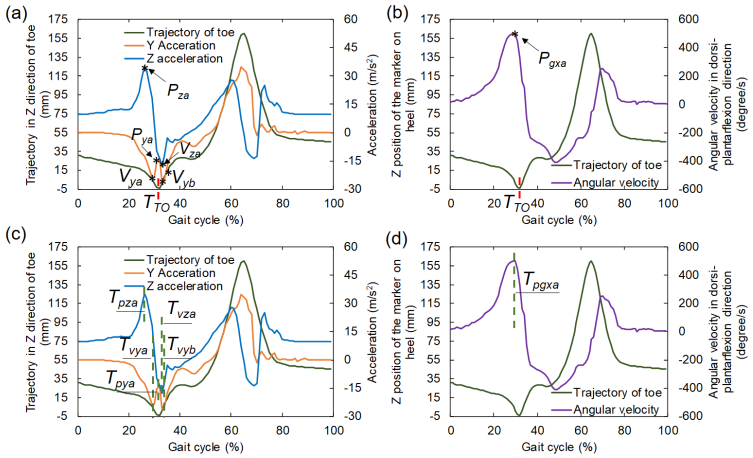

Fig. 5 (a) Trajectory of toe and synchronized Y & Z acceleration waveforms. (b) Trajectory of toe and synchronized angular velocity waveform in dorsalflexion/plantarflexion direction. (c) Timing of selected candidate features of TO in Y & Z acceleration waveforms. (d) Timing of selected candidate feature of TO in angular velocity waveform in dorsalflexion/plantarflexion direction.

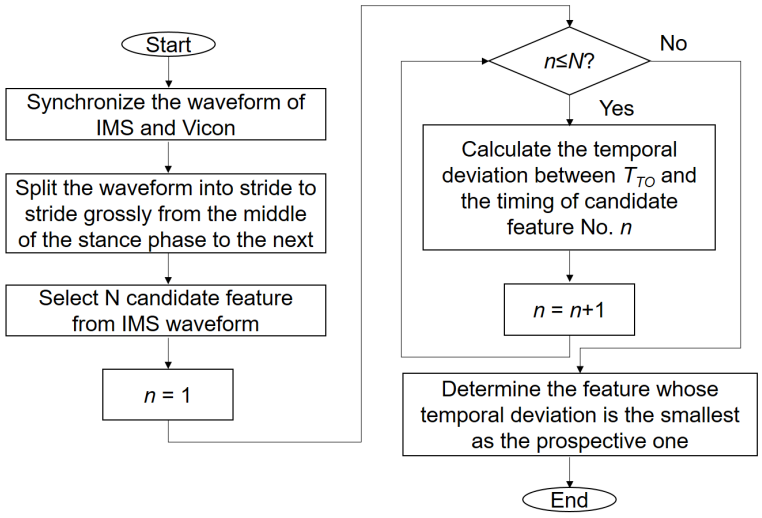

Fig. 6 Flow chart of prospective feature determination.

Table 1 Six candidate timing points of TO.

Candidate timing of TO	Description
T_{pza}	The timing of P_{za}.
T_{pgxa}	The timing of P_{gxa}.
T_{vya}	The timing of V_{ya}.
T_{pya}	The timing of P_{ya}.
T_{vza}	The timing of V_{za}.
T_{vyb}	The timing of V_{yb}.

A flow chart for extracting candidate TO features is shown in Fig. 7. According to the characteristics of IMS signals, first, the first half of waveforms L_y, L_z, or L_{gx} are indicated as L_{y1}, L_{z1}, or L_{gx1}. V_{ya} and V_{yb} are determined by inversing L_{y1} by using the peak detection function in MATLAB. The first and second peaks in the inversed L_{y1}, i.e., the first and second valleys in L_{y1}, are indicated as V_{ya} and V_{yb}, and their timings are indicated as T_{vya} and T_{vyb}. To exclude the influence of noise, we chose a condition in which only peaks whose prominence is over $3\,\mathrm{m/s^2}$ are able to be recognized. Then, the local maximum of the waveform between V_{ya} and V_{yb} is P_{ya}, whose timing is indicated as T_{pya}. The maximum and minimum of L_z are indicated as P_{za} and V_{za}, and their timings are indicated as T_{pza} and T_{vza}. The maximum of L_{gx} is indicated as P_{gxa}, and its timing is indicated as T_{pgxa}. As a result, a total of six candidate timing-points were selected, and they are listed in Table 1.

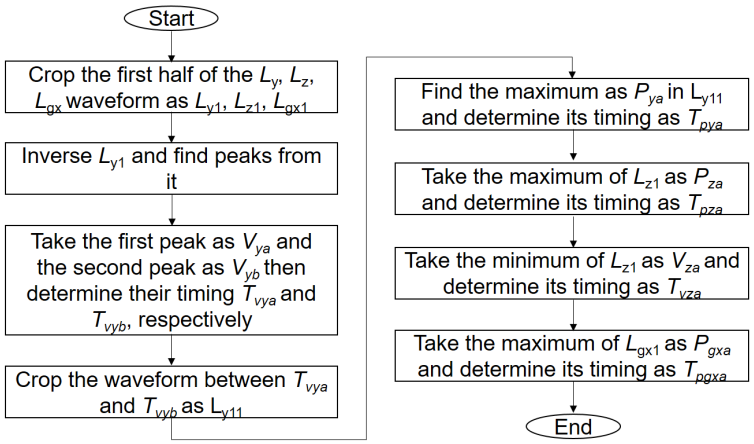

Fig. 7 Flowchart of candidate TO features extraction.

2.5.2 IC detection

An example of synchronized Y and Z acceleration waveforms Ly and Lz and the trajectory in the Z direction of the marker on the heel are combined in Fig. 8(a) and (c), and the synchronized angular velocity waveform in the dorsalflexion/plantarflexion direction L_{gx} and the trajectory in the Z direction of the marker on the heel are combined in Fig. 8(b) and (d). Observing the signals, it can be seen that no characteristic features like peaks, valleys, or turning points appeared at the moment of T_{IC} in L_y, L_z, or L_{gx}. It can be seen that T_{IC} appeared just after P_{yb} and V_{zb} in Fig. 8(a) and before P_{zb}, P_{gxb} and V_{yc} in Fig. 8(b). Although, where the prospective feature of IC is or whether the prospective feature belongs to one of these five characteristic features cannot be confirmed at this stage, they are considered to be candidates, and the prospective feature should be in this limited range. We determine the prospective feature of IC by using the same process as TO feature determination.

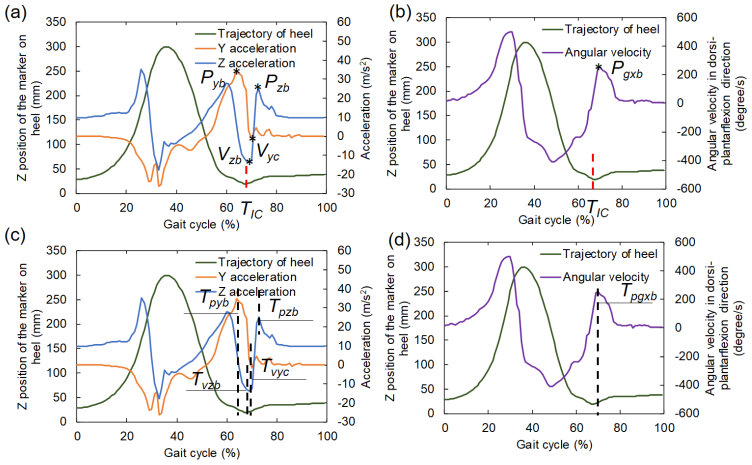

Fig. 8 (a) Trajectory of heel and synchronized Y & Z acceleration waveforms. (b) Trajectory of heel and synchronized angular velocity waveform in dorsalflexion/plantarflexion direction. (c) Timing of selected candidate features of IC in Y & Z acceleration waveforms. (d) Timing of selected candidate feature of IC in angular velocity waveform in dorsalflexion/plantarflexion direction.

A flow chart for extracting candidate IC features is shown in Fig. 9. First, the second half of waveforms L_y, L_z, or L_{gx} are indicated as L_{y2}, L_{z2} or L_{gx2}. The maximum of L_{y2} is indicated as P_{yb}, the minimum of L_{z2} is indicated as V_{zb}, the maximum of L_{gx2} is indicated as P_{gxb}, and the maximum of L_{z2} is indicated as P_{zb}. It is observed that a valley V_{yc} is also a characteristic point in a curve. The slope of the curve suddenly changes after passing through V_{yc} so that V_{yc} can be treated as a significant turning point. Here, the triangle thresholding algorithm [20] is applied for determining V_{yc} from a cropped partial waveform, which is cropped from L_{y2}. The timings of P_{yb}, V_{zb}, P_{zb}, P_{gxb}, and V_{yc} are marked as T_{pyb}, T_{vzb}, T_{pzb}, T_{pgxb},

Table 2 Six candidate timing points of TO.

Candidate timing of IC	Description
T_{pyb}	The timing of P_{yb}.
T_{vzb}	The timing of V_{zb}.
T_{pgxb}	The timing of P_{gxb}.
T_{pzb}	The timing of P_{zb}.
T_{vyc}	The timing of V_{yc}.

and T_{vyc}, respectively. As a result, a total five candidate timing points are selected as candidate IC timing. Five candidate timing points are listed in Table 2.

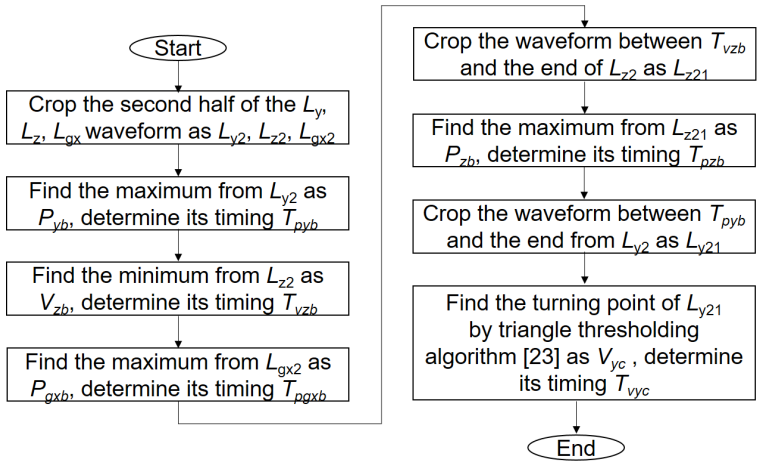

Fig. 9 Flowchart of candidate IC feature extraction.

2.6 Statistical analysis

All strides except the first and last in one trial were included in the data set for statistical analysis, and the signals induced by obvious abnormal walking were also excluded from the data. Finally, a total of 425 strides were used for analysis. The timing of the TOs and ICs was automatically extracted by the algorithm mentioned above. The results obtained from the Vicon data were used as real values for reference.

The mean value and standard deviation (SD) of the temporal deviations between T_{TO} or T_{IC} and the timing of each selected feature were calculated, and the temporal deviations were also evaluated on the basis of root mean square error (RMSE). Levels of agreement between them are expressed as intraclass correlation coefficients (ICCs)

Table 3 Results of TO feature determination.

Candidate timing of TO	Mean ± SD (ms)	RMSE in time (ms)	RMSE in %	r	ICC(2, k)
T_{pza}	-41.2 ± 12.4	43.0	3.96%	0.5327*	0.1443
T_{pgxa}	-7.5 ± 16.4	18.1	1.66%	0.4616*	0.5741
T_{vya}	**3.3 ± 15.0**	**12.9**	**1.22%**	**0.5571***	**0.7011**
T_{pya}	23.0 ± 12.9	26.4	2.47%	0.5181*	0.3635
T_{vza}	41.7 ± 17.7	45.3	4.22%	0.3349*	0.1338
T_{vyb}	49.3 ± 16.3	51.9	4.84%	0.4114*	0.1239

*p<0.05

Table 4 Results of IC feature determination.

Candidate timing of TO	Mean ± SD (ms)	RMSE in time (ms)	RMSE in %	r	ICC(2, k)
T_{pyb}	-30.0 ± 38.6	48.9	4.43%	0.1158*	0.1085
T_{vzb}	-25.9 ± 19.5	32.4	2.92%	0.3677*	0.2921
T_{pgxb}	24.0 ± 19.9	31.1	2.83%	0.5030*	0.4361
T_{pzb}	33.1 ± 19.4	32.4	2.92%	0.4935*	0.3191
T_{vyc}	**5.4 ± 14.2**	**15.3**	**1.40%**	**0.6589***	**0.7721**

*p<0.05

of type (2, k). The Pearson product-moment (r) was also calculated to measure the linear correlation between them. Independent t-tests were used to examine the difference between groups. For all analyses, statistical significance was set at p<0.05. A predefined acceptance rating similar to the previous recommendations for ICCs were set at excellent (>0.900), good (0.750-0.899), fair (0.500-0.749), and poor (<0.500) [21].

3 Results

By calculating the (Mean ± SD) and the RMSE between T_{TO} or T_{IC} and the timing of each selected feature, the prospective features were able to be determined. The results of evaluating TO determination, including the (Mean ± SD), the RMSE in terms of time and percentage for one normalized gait cycle, r, and ICC(2, k) are shown in Table 3. The results of evaluating IC determination are shown in Table 4.

Comparing the evaluation timings of the listed candidate features of TO, T_{vya} was the nearest and had the smallest temporal deviation and biggest r and ICC(2, k) from the Vicon-measured TO timing. This means that the timing at which V_{ya} appeared, that is, the first valley of the “W” shape wave pattern appearing after each middle-stance phase in the acceleration signal in the anterior-posterior direction, should be the timing of TO. The observer variation and agreement between the Vicon- and IMS-measured T_{vya} are shown in Fig. 10(a). Although several points were

Table 5 Six candidate timing points of TO.

Gait event	Feature in IMS signal
TO	The first valley of a "W" shape wave pattern appears after each middle stance phase in the acceleration signal in the anterior-posterior direction.
IC	A sharp valley appearing next to the maximum of acceleration in the anterior-posterior direction in each gait cycle.

distributed far away from the equivalent line, most of the points (including many points overlapping with each other) were concentrated around the line. The ICC(2, k) value of T_{vya} indicates that if we take values measured by 3-D motion capture as the gold standard, using V_{ya} to detect a TO event when applying IMS for gait analysis has the nearly “ good ” effect of a deviation of only 13.2 ms and 1.24

Comparing the evaluation timings of the listed candidate features of IC, T_{vyc} was the nearest and had the smallest temporal deviation and biggest r and ICC(2, k) from the Vicon-measured IC timing. This means that the timing at which V_{yc} appeared, that is, a sharp valley appearing next to the maximum of acceleration in the anterior-posterior direction in each gait cycle, should be the timing of IC. The observer variation and agreement between the Vicon- and IMS-measured T_{vyc} are shown in Fig. 10(b). Almost all of the points were concentrated on or near the equivalent line. The ICC(2, k) value of T_{vyc} indicates that using V_{yc} to detect an IC event when applying IMS for gait analysis has a “ good ” effect. There was a deviation of only 15.3 ms and 1.40

Finally, the IMS features determined for TO and IC detection are summarized in Table 5.

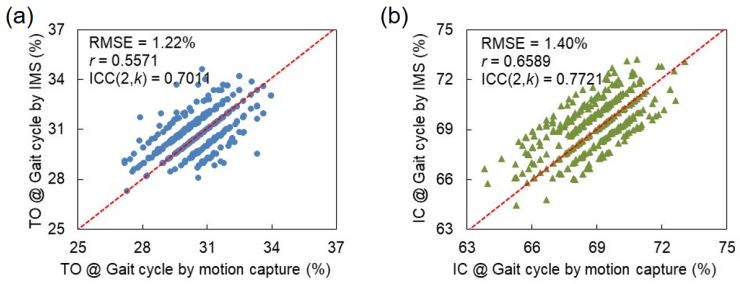

Fig. 10 (a) Observer variation and agreement of TO. (b) Observer variation and agreement of IC.

4 Discussion

The patterns in gait signals should be intrinsically induced by the human walking mechanism. In this study, the significant features of TO and IC were both found in acceleration waveforms in the anterior-posterior direction (Y acceleration). The feature of TO was considered to be induced in the process of transitioning from the stance phase to the swing phase. Figure 11 shows a schematic of this transition process and explains the principle of the double valley occurrence. At the end of the pre-swing phase, a motion called a “forefoot rocker” [22] occurs, indicating the rotation of the metatarsophalangeal joint after heel rising. Because the position of the foot arch deviates from the rotation axis of the metatarsophalangeal joint, the rotation moment during the forefoot rocker motion contributes to acceleration Wfr in the tangent direction there until the toe departs from the ground. In this process, the calf muscle provides the propulsion power to move forward and continuously increases the power until TO. Hence, the composition in the Y direction Y_{fr} increases continuously in the anterior direction. Then, at the beginning of the initial swing phase, the lower limb needs to be pushed forward, and acceleration in the anterior direction W_{sw} is stilled maintained. However, during this transition process, the propulsion power of the lower limb transitions from the calf muscle and friction force of the ground to the rectus femoris at the exact moment of the toe-off event [18, 23-25]. Due to the muscle activation transition, the instantaneous propulsion power decreases, which causes the acceleration to decrease and consequently generates the first valley V_{ya} in the early phase of Y acceleration. Finally, after the rectus femoris is activated, a second propulsion induces a second acceleration rise in the anterior direction that forms a peak P_{ya} between V_{ya} and V_{yb}. The results also mean that the transition process of muscle activation during walking is detected by the IMS.

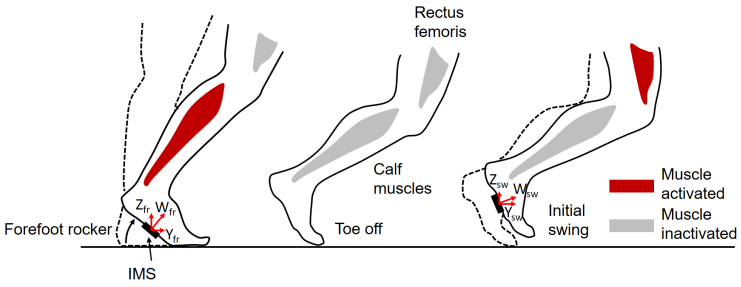

Fig. 11 Transition process from pre-swing phase to initial swing phase.

The feature of IC is a sharp valley appearing next to the maximum of the acceleration in the anterior-posterior direction in each gait cycle. In fact, at the end of the terminal swing phase, the lower limb decelerates in a short while to prepare the heel strike [22], which is the origin of P_{yb} and V_{zb}. On the other hand, a motion called a

“heel rocker” exists after the heel strike and before the sole landing. It is a rotation motion of the ankle joint lasting several milliseconds [26] and corresponding to V_{yc}. Figure 12 shows a schematic of the heel rocker motion and explains the origin of V_{yc}. Because the position of the foot arch also deviates from the extended center axis of the tibia and the rotation axis of the ankle joint, the IMS under the foot arch detects acceleration W_{hr} in the tangent direction induced by the rotation moment during the heel rocker motion. When an IC occurs, a sudden heel rocker provides W_{hr}, and W_{hr} then produces acceleration in the anterior direction whose direction is opposite the acceleration immediately before the IC. As a result, the sudden change in acceleration vector induces the feature of IC. Although Jagos et al. [26] suggested that P_{yb}, i.e., the timing of the biggest deceleration of the lower limb, might be the feature of IC, according to our results, there was no inevitable connection between P_{yb} and IC.

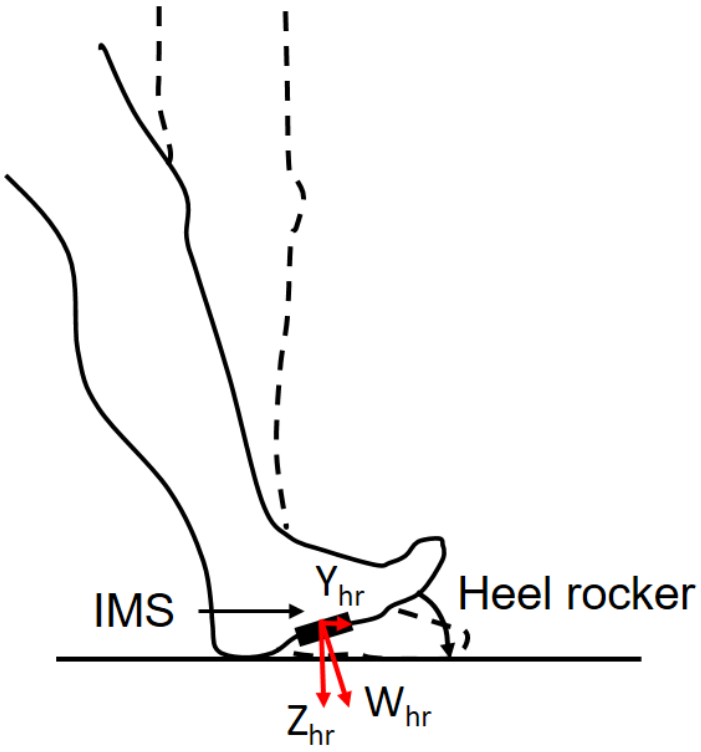

Fig. 12 Schematic of heel rocker motion as origin of V_{yc}.

Mannini et al. [27] successfully detected TO and IC gait events by using an HMM model with a precision of 15 ms and 32 ms. They also used a 3D-motion analysis system as a reference rater. The results in this study indicate that it is more accurate

to detect TO and IC events by specifying the waveform features from gait signals on the basis of biomechanical knowledge, which proves that our method is effective. The temporal deviation is thought to be due to two reasons. The noise of the motion sensor should be the first reason. Noise peaks may lead to wrong output in the peak detection process. Second, due to the occasionally weak Bluetooth connection between the IMS sensor and smartphone user interface, data packets were lost during the communication, which induced tiny deviations between the motion sensor and Vicon waveform in the later part of the data stream. Therefore, as a solution for improving the precision, after splitting the data stream, the waveforms of each stride of IMS and Vicon can be synchronized again by making their peaks and valleys in the sole-to-ground angle in the dorsal-flexion/plantar-flexion waveform uniform. If the Bluetooth connection state were improved, the precision should be higher.

In some previous studies [16, 26, 28], foot pressure signals obtained with force plates or foot pressure sensors were chosen as the reference rater for determining the reference gait-event timing by setting a threshold intensity for foot pressure. However, the timing when the pressure signal exceeded the threshold was determined to be IC, and the timing when the pressure signal fell below the threshold was determined to be TO. As the result, the determined timing of IC is actually behind the real IC, and that of TO is actually before the real TO. Furthermore, the reference is unstable due to threshold change or individual weight differences. Some researchers suggested that using 3D motion analysis systems to measure the spatial locations of the heel and toe would more greatly help in approaching the real timing of TO and IC according to their original definition [21, 27, 29].

5 Conclusion

In this study, foot to ground kinematic temporal features measured beneath the foot arch at the time of TO and IC events were discovered by synchronizing an IMS and Vicon 3-D motion analyzer. Thanks to these biomechanical knowledge based-signal features that are easy to recognize, we achieved a simpler method for detecting gait events for IMS systems by specifying the events from gait signals obtained by IMS. Furthermore, the evaluation results demonstrated that our method had a higher TO and IC detection accuracy than the previous ones. The reliability of this algorithm was also confirmed on the basis of the good agreement of the IC and TO measured timings between the IMS and Vicon. These discovered features have the potential of being used for a standard gait-event detection method used for daily gait analysis for healthy subjects with an in-shoe sensor.

References

1. Hodgins, D.: The importance of measuring human gait. Med. Device. Technol., **19**, 44–47 (2008).
2. Keijsers, N.L., Horstink, M.W. and Gielen, S.C.: Ambulatory motor assessment in Parkinson disease. Movement Disord. **21**, 34–44 (2006).
3. Hausdorff, J.M., Lertratanakul, A., Cudkowicz, M.E., Peterson, A.L., Kaliton, D, and Goldberger, A.L.: Dynamic markers of altered gait rhythm in amyotrophic lateral sclerosis. J. Appl. Physiol. **88**, 2045–2053 (2000).
4. Hausdorff, J.M., Rios, D.A. and Edelberg, H.K.: Gait variability and fall risk in community-living older adults: A 1-year prospective study. Arch. Phys. Med. Rehab. **82**, 1050–1056 (2001).
5. Neumann, D.A.; in *Kinesiology of the musculoskeletal system: foundations of physical rehabilitation, Second Edition*, (Mosby, St Louis, MO, USA, 2010), p. 636–650.
6. Morris, M.E., Matyas, T.A., Iansek, R. and Summers, J.J.: Temporal stability of gait in Parkinson's disease. Phys. Ther. **76**, 763–777 (1996).
7. Ornetti, P., Maillefert, J.F., Laroche, D., Morisset, C., Dougados, M. and Gossec, L.: Gait analysis as a quantifiable outcome measure in hip or knee osteoarthritis: a systematic review. Joint Bone Spine **77**, 421–425 (2010).
8. Whittle, M.W.: Clinical gait analysis: A review. Hum. Mov. Sci. **15**, 369–387 (1996).
9. MacDonald, C., Smith, D., Brower, R., Ceberio, M. and Sarkodie-Gyan, T.: Determination of human gait phase using fuzzy inference. In *Proceedings of 10th IEEE International Conference on Rehabilitation Robotics*, (Noordwijk, The Netherland, 13—15 June 2007), p. 421–425.
10. Lau, H. and Tong, K.: The reliability of using accelerometer and gyroscope for gait event identification on persons with dropped foot. Gait Posture **27**, 248–257 (2008).
11. Gouwanda, D. and Gopalai, A.A.: A robust real-time gait event detection using wireless gyroscope and its application on normal and altered gaits. Med. Eng. Phys. **37**, 219–225 (2015).
12. Stamatakis, J., Cremers, J., Maquet, D., Macq, B. and Garraux, G.: Gait feature extraction in Parkinson's disease using low-cost accelerometers. In *Proceeding of 2011 Annual International Conference of the IEEE Engineering in Medicine and Biology Society*, (Boston, MA, USA, 30 August–3 Sept. 2011), p. 7900–7903. (2011).
13. Williamson, R. and Andrews, B.J.: Gait event detection for FES using accelerometers and supervised machine learning. IEEE Trans. Rehabil. Eng. **8**, 312–319 (2000).
14. Mannini, A. and Sabatini, A.M.: A hidden Markov model-based technique for gait segmentation using a foot-mounted gyroscope. In *Proceedings of 2011 Annual International Conference of the IEEE Engineering in Medicine and Biology Society*, (Boston, MA, USA, 30 August–3 September 2011), p. 4369–4373.
15. Jung, P.G., Oh, S., Lim, G. and Kong, K.: A mobile motion capture system based on inertial sensors and smart shoes. In *Proceeding of 2013 IEEE International Conference on Robotics and Automation*, (Karlsruhe, Germany, 6-10 May 2013), p. 692–697.
16. Jagos, H., Pils, K., Haller, M., Wassermann, C., Chhatwal, C., Rafolt, D. and Rattay, F.: Mobile gait analysis via eSHOEs instrumented shoe insoles: A pilot study for validation against the gold standard GAITRite®. J. Med. Eng. Technol. **41**, 375–386 (2017).
17. Mijailović, N.; Gavrilović, M.; Rafajlović, S.; Đurić-Jovičić, M. and Popović, D.: Gait phases recognition from accelerations and ground reaction forces: Application of neural networks. Telfor J. **1**, 34–36 (2009).
18. Endo, K. and Herr, H.: Human walking model predicts joint mechanics, electromyography and mechanical economy. In *Proceeding of 2009 IEEE/RSJ International Conference on Intelligent Robots and Systems*, (St. Louis, MO, USA, 10–15 October 2009), p. 4663-4668.
19. Madgwick, S.: An efficient orientation filter for inertial and inertial/magnetic sensor arrays. Report x-io and University of Bristol (UK) **25**, 113–118 (2010).
20. Nilufar, S.; Morrow, A.A.; Lee, J. M. and Perkins, T.J.: FiloDetect: automatic detection of filopodia from fluorescence microscopy images. BMC Syst. Boil. **7**, 66 (2013).

21. Hartmann, A., Luzi, S., Murer, K., deBie, R.A. and de Bruin. E.D.: Concurrent validity of a trunk tri-axial accelerometer system for gait analysis in older adults. Gait Posture **29**, 444–448 (2009).
22. Abu-Faraj Z.O., Harris G.F., Smith P.A. and Hassani S.: Human Gait and Clinical Movement Analysis. in *Wiley Encyclopedia of Electrical and Electronics Engineering, Second Edition*, (John Wiley & Sons, Inc., New York, USA, 2015), p. 1–34.
23. Takahashi, K.Z., Gross, M.T., Van Werkhoven, H., Piazza, S.J. and Sawicki, G.S.: Adding stiffness to the foot modulates soleus force-velocity behaviour during human walking. Sci. Rep. **6**, 29870 (2016).
24. Nene, A., Mayagoitia, R. and Veltink, P.: Assessment of rectus femoris function during initial swing phase. Gait Posture **9**, 1–9 (2009).
25. Farris, R.J., Quintero, H.A., Withrow, T.J. and Goldfarb, M.: Design of a joint-coupled orthosis for FES-aided gait. In *Proceedings of 2009 IEEE International Conference on Rehabilitation Robotics*, (Kyoto, Japan, 23–26 June 2009), p. 246–252.
26. Jagos, H., Reich, S., Rattay, F., Mehnen, L., Pils, K., Wassermann, C., Chhatwal, C. and Reichel, M.: Determination of gait parameters from the wearable motion analysis system eSHOE. Biomed. Tech. **58**, Issue SI-1-Track-K (2013).
27. Mannini, A. and Sabatini, A.M.: Gait phase detection and discrimination between walking-jogging activities using hidden Markov models applied to foot motion data from a gyroscope. Gait Posture **36**, 657–661 (2012).
28. Mariani, B., Rouhani, H., Crevoisier, X. and Aminian, K.: Gait phase detection and discrimination between walking-jogging activities using hidden Markov models applied to foot motion data from a gyroscope. Gait Posture **37**, 229–234 (2013).
29. Evans, R.L. and Arvind, D.K.: Detection of gait phases using orient specks for mobile clinical gait analysis. In *Proceedings of 2014 11th International Conference on Wearable and Implantable Body Sensor Networks*, (Zurich, Switzerland, 16–19 June 2014), p. 149-154.